Bioprinting xxx (xxxx) xxx

Contents lists available at ScienceDirect

Bioprinting

journal homepage: www.elsevier.com/locate/bprint

Comparative characterization of the hydrogel added PLA/β-TCP scaffolds produced by 3D bioprinting

Mehmet Onur Aydogdu [a], Ebru Toksoy Oner [b], Nazmi Ekren [a,c], Gokce Erdemir [d], Serap Erdem Kuruca [e], Esra Yuca [f], Muge Sennaroglu Bostan [g], Mehmet S. Eroglu [g], Fakhera Ikram [h], Muhammet Uzun [a,i], Oguzhan Gunduz [a,j,*]

[a] Center for Nanotechnology & Biomaterials Research, Marmara University Goztepe Campus, 34722, Istanbul, Turkey
[b] Department of Bioengineering, Faculty of Engineering, Marmara University Goztepe Campus, 34722, Istanbul, Turkey
[c] Department of Electrical and Electronics Engineering, Marmara University, Goztepe Campus, 34722, Istanbul, Turkey
[d] Institute of Aziz Sancar Experimental Medicine Research, Faculty of Medicine, Istanbul University, 34093, Fatih, Istanbul, Turkey
[e] Department of Physiology, Istanbul University, Capa, 34393, Istanbul, Turkey
[f] Department of Molecular Biology and Genetics, Yildiz Technical University, Istanbul, Turkey
[g] Department of Chemical Engineering, Faculty of Engineering, Marmara University, Goztepe Campus, 34722, Istanbul, Turkey
[h] Interdisciplinary Research Centre in Biomedical Materials, COMSATS University Islamabad, Lahore Campus, Defence Road, Off Raiwind Road, Lahore, Pakistan
[i] Department of Textile Engineering, Faculty of Technology Marmara University Goztepe Campus, 34722, Istanbul, Turkey
[j] Department of Metallurgical and Materials Engineering, Faculty of Technology Marmara University Goztepe Campus, 34722, Istanbul, Turkey

ARTICLE INFO

Keywords:
Polylacticacid
β-tricalcium phosphate
Hydrogels
3D bioprinting
Tissue engineering

ABSTRACT

Designing the 3D bioprinted scaffolds has been a promising tool which assists cells to adhere and supports the self-repair mechanism of native tissues. In order to practice this hypothesis, we used 3D bioprinting methods and fabricated Polylactic acid (PLA) and β-tricalcium phosphate (β-TCP) scaffolds and incorporated them with four different hydrogels (Collagen (Col), Sodium Alginate (SAlg), Halamomas Levan (HLh), Chitosan (Ch). Furthermore, PLA/β-TCP Scaffolds incorporated with chitosan were further enhanced with Amoxicillin (AMX). These scaffolds were further characterized for their chemical, morphological, antibacterial and cellular biocompatibility. Scanning electron microscopy (SEM), Fourier transform infrared spectroscopy (FTIR), differential scanning calorimetry, compressive strength test, agar diffusion test and in vitro cellular behaviour tests were performed to reveal structural, mechanical and biological characteristics of scaffolds. Among others, chitosan including samples demonstrated significantly superior and beneficial features such as the highest biocompatibility and structural integrity regarding morphology, compared to the other samples. Therefore, chitosan including samples were loaded with amoxicillin (AMX) to increase antimicrobial activity of the scaffolds. All together, these data show that PLA/β-TCP 3D printed scaffolds incorporated with different hydrogels has the ability to assist the tissue to repair and regeneration.

1. Introduction

Reports are showing that the most commonly used way to compensate the organ or tissue damages is the transplantation of the related tissue or organ. In the USA, an average number of people received organ transplants each day is 79, on the contrary, morbidity rates due to unavailability of organ transplantation are 18 people per day [1]. Due to certain limitations of the organ transplantation such as immunological rejection and lack of donors, researchers were forced into developing a new method of treatment which should not be demanding and expensive. Therefore, tissue engineering studies have been extended very comprehensively from the year it was first introduced as the development of biological substitutes that restore, protect or develop tissue functions in 1993 by Langer and Vacanti [2]. As a favourite multidisciplinary branch of the regenerative science, tissue engineering consisted by a blend of widespread practices of biology, material science, chemistry, molecular biology, engineering and medicine by combining native cells, biocompatible materials and bioactive molecules in order to create functional three-dimensional tissue scaffolds to overcome related problems such as organ or tissue damage [3]. Primary constituents of tissue scaffolds

* Corresponding author. Center for Nanotechnology & Biomaterials Research, Marmara University Goztepe Campus, 34722, Istanbul, Turkey.
E-mail address: ucemogu@ucl.ac.uk (O. Gunduz).

https://doi.org/10.1016/j.bprint.2019.e00046
Received 24 December 2018; Received in revised form 14 February 2019; Accepted 3 March 2019
2405-8866/

concept are the production of porous morphological structures with increased surface ratio and usage of biocompatible materials during this production in order mimic extracellular matrix (ECM) of the native tissues and providing a suitable environment for cells to attach and proliferate as well as having certain levels of biocompatibility [4,5].

Traditional methods such as electrospinning and freeze-drying were successfully implemented to build tissue scaffolds [6,7]. However, conventional approaches have led the scientist into specific difficulties such as maintaining the morphological integrity of the scaffolds and uncontrollable scaffold microstructures [8]. Therefore, a new technique called 3D bioprinting, also known as additive manufacturing (AM), was emerged rapidly to overcome the problems of the other manufacturing methods in recent years by enabling a higher degree of control over architecture and geometry of the scaffolds [9]. It can be defined as layer by layer production method of three-dimensional materials from 3D models previously designed with computer-aided software [10]. Material selection is also another critical aspect of developing adequate tissue scaffolds. Owing to the certain requirement for biocompatibility, tissue scaffolds need to be consisted by biomaterials to provide desirable tissue response and to be able to contribute the native ECM of the target tissue [11,12]. One of the most commonly used and most effective methods for material selection is blending synthetic polymers with natural polymers. Various studies were already published for skin, bone, cartilage tissues and artificial blood vessels combining those two variations of the polymers and creating biocompatible scaffolds [13–16].

Polylactic acid (PLA) is a non-toxic, biocompatible and biodegradable synthetic polymer with a long history of safe medical use [17]. It has been already used in various studies including bone tissue engineering studies and reported with good outcomes in both in vitro and in vivo [18]. However, due to relatively low mechanical properties of PLA, an accompanying material can be beneficial to be used along with PLA to design better scaffolds. Consequently, a composite material will be obtained and scaffolds can benefit from individual favourable properties of both materials [19]. Beta tricalcium phosphate (β-TCP) as one of the most popular calcium phosphate ceramics is well known material by their synergy with environmental tissues and ability to induce osteoconductivity as well as their proven and successful contribution in various studies of bone tissue engineering [20]. Therefore, due to high mechanical properties and exceptional bone remodelling capacity, β-TCP can be useful to be used along with PLA polymer to create tissue scaffolds [21]. Hydrogels are also considered as a promising material for constructing the tissue scaffolds since they can provide remarkable features such as the ability to provide nutrient and waste interchange and ability to stimulate the formation of a suitable environment for the cell to attach [22]. Collagen (Col) has become popular with its remarkable biocompatibility since it's one of the main constituents of ECM in bone, tendon, ligament, skin, muscle tissues [23]. Levan (HLh) is a nontoxic and antioxidant polysaccharide, which can improve the biocompatibility in composite material structure [24]. As a hydrophilic, biocompatible polymer, sodium alginate (SAlg) is mostly known for their biomedical and pharmaceutical practices. It has been reported that the sodium alginates can enhance the cell proliferation and therefore, they can increase the biocompatibility [25]. Chitosan (Ch), a polysaccharide that is originated mostly from the crab shells and reported with no toxicity and good biodegradability, has become very popular and an excellent candidate to be used in tissue engineering studies [26–28]. As an antimicrobial material, Amoxicillin (AMX), a broad-spectrum antibiotic, acting as an antimicrobial barrier and being effective against many pathogens and used within the scaffolds produced for tissue engineering studies [29,30].

In the present work, PLA polymer blended with β-TCP ceramic and this composite structure was enhanced with different types of hydrogels (Collagen (Col), Sodium Alginate ((SAlg), Halamomas Levan ((HLh), Chitosan (Ch) and scaffold fabricated with Chitosan (Ch) were also enhanced with AMX to determine and compare antibacterial properties of the scaffolds These scaffolds were characterized for chemical, morphological, antibacterial features and cellular behaviour.

2. Experimental details

2.1. Materials

Poly (L-lactide) (PLA), Human Collagen (Bornstein and Traub Type I, recombinant, expressed in Nicotiana tabacum), Sodium Alginate, Gelatin and Chitosan, were purchased from Sigma- Aldrich. Beta-Tricalcium Phosphate (β-TCP), Dichloromethane (DCM) and Dimethyl sulfoxide (DMSO) were supplied from Merck. For cell viability assays, Saos-2 (human osteosarcoma) cell lines were used obtained from The American Type Culture Collection (ATCC). Dulbecco's modified Eagle medium (DMEM) and Fetal Bovine Serum (FBS) was purchased from Gibco. *Halomonas* levan hydrogel was obtained from Industrial Biotechnology and Systems Biology Research Laboratory (Marmara University, Istanbul, Turkey).

2.2. Preparation of the polymer/hydrogel blend solutions

A composite matrix which consists of a ceramic and a polymer phase was prepared. They were identified by the weight content (wt. %) of polymer and ceramic phases with 10: 5 PLA: β-TCP ratio. DCM was used as a dissolving agent at ambient temperature (23 °C) to provide sufficient and rapid evaporation rate for proper solidification of the scaffolds. Once dissolving PLA and β-TCP in DCM, first scaffold candidate that will be used was obtained. After that, binary blends of PLA- β-TCP was enhanced with five different hydrogels (Col, HLh, SAlg, and Ch) 1 wt % concentration ratio individually. Four samples including hydrogel and one without hydrogel was obtained. Finally, a final blend was created by mixing four different components which are PLA, β-TCP, Ch and AMX. Each blend was prepared individually after required calculations in order to maintain the chosen material concentrations. Solution was appropriately stirred using a magnetic stirrer (WiseStir®, MSH-20A, Germany) for 30 min at 35 °C.

2.3. Scaffold fabrication

Before the 3D Bioprinting, scaffold morphology was determined using CAD software (SolidWorks). The three-dimensional (3D) structure of the scaffolds was fabricated with an exceptional 3D Bioprinting System (Hyrel 3D, SDS-5 Extruder, GA, USA), using 0°/90° architecture. Fig. 1 consists of a camera images of the (Fig. 1a.) 3D bioprinter used in this study (Fig. 1b.), bioprinting process (Fig. 1b_1.), and 3D bioprinted scaffold along with the (Fig. 1c.) schematic illustration of the 3D bioprinting process and layer by layer production mechanism of the scaffolds. Solutions were loaded into 10 mL Luer lock syringe that is directly connected to stainless steel luer nozzle with 0.81 mm outer diameters. The flow rate during the bioprinting was controlled by digital syringe pump module of the 3D bioprinter, which was set to 1 ml/h 3D Bioprinting was optimized at 50 mm/s printing speed. This methodology was repeated for each type of hydrogel type used in this study and scaffolds were prepared using same parameters in similar environmental conditions to prevent scaffolds to be affected by any other factors but the material type used in the study. Right after production, sodium hydroxide were sprayed on scaffolds and then scaffolds were treated within CO_2 incubator with the purpose of supporting the crosslink mechanism of the hydrogels.

2.4. Characterization

2.4.1. Characterization of the solution properties

To maintain repeatability of the experiments conducted in this study, viscosity, density, and surface tension of all blend solutions were determined. Viscosity was measured using a Brookfield (DV-E, Massachusetts, USA) viscometer at 10 rpm under ambient temperature over 120 s. The surface tension of the solutions was determined by a Sigma 700, (DYNE,

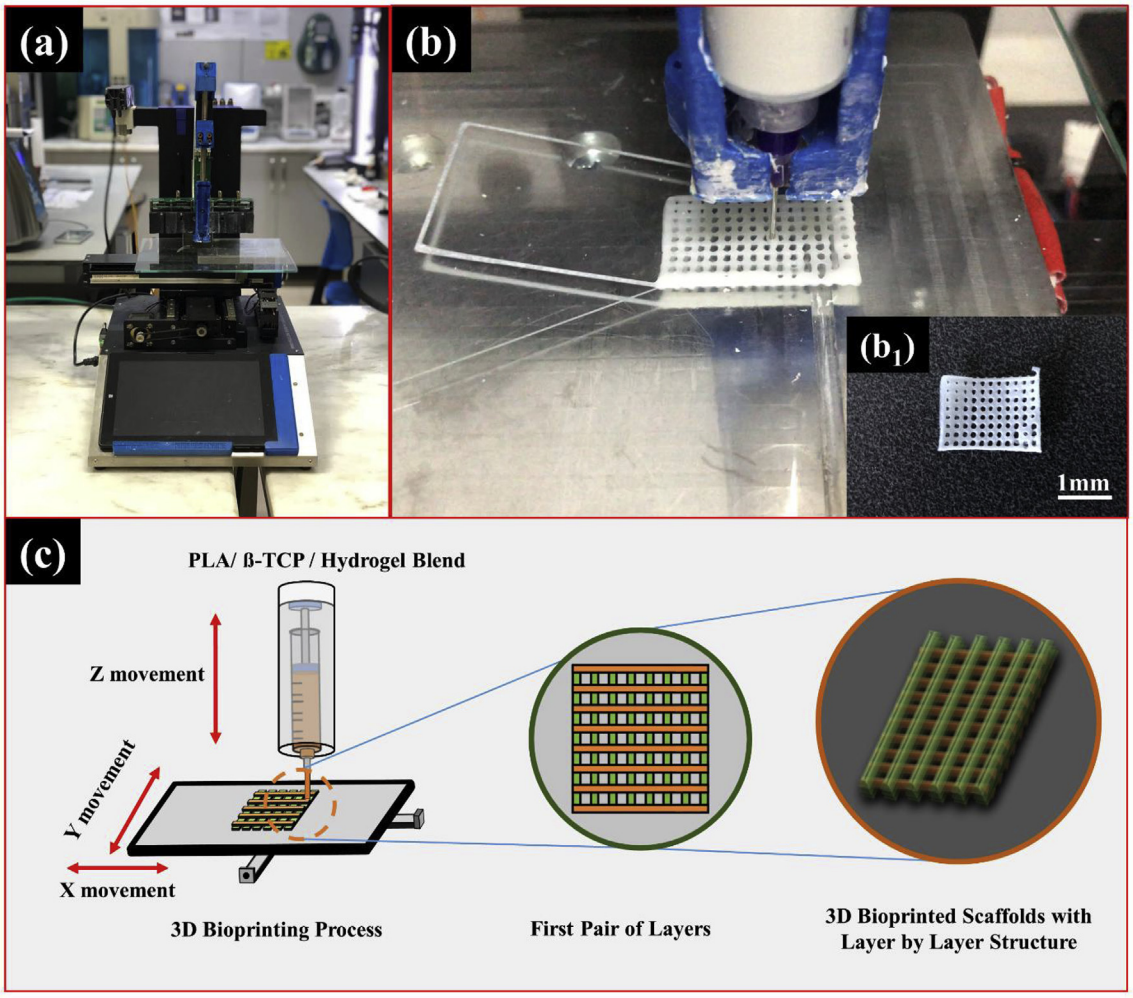

Fig. 1. Camera image of the (a) 3D bioprinter, (b) scaffold during bioprinting, (b_1) scaffold after bioprinting along with the (d) schematic illustration of the 3D bioprinting and layer by layer manufacturing method.

UK) tensiometer. Each equipment used in this study was calibrated before the use, and each test was carried out five times at room temperature (23 °C) and a relative humidity of 45–50%. Density was measured using a standard 10 mL density bottle.

2.4.2. Scaffold morphology and structural integrity

To analyse the morphology of the scaffolds, an EVO MA-10 Scanning Electron Microscope (SEM, Carl Zeiss, OR, USA) was used. Surface morphology of the scaffolds was revealed at an accelerating voltage of 5 kV. Prior to the SEM imaging, scaffolds were sputter-coated with gold using a sputter coating machine (Quorum SC7620, USA) for 60s to obtain 18.35 µm of thickness. Each scaffold was analysed for morphological differences and structural integrity. Average diameters of the gaps within the scaffolds were determined by performing 100 random measurements using a software (Analysis5, Olympus, USA) and maximum, minimum and mean diameter values were calculated for each sample. Mechanical properties were obtained by uniaxial compression test.

2.4.3. Mechanical properties of the scaffolds

A universal testing machine DVT (Devotrans, Istanbul, Turkey) with a 45 kN load cell was used. Crosshead velocity was set to 1 mm/min. Each type of scaffold was subjected to the compression test. Prior to the test, the surface area of the samples was measured using digital clipper (500, Mitutoyo, USA).

2.4.4. Biodegradation and Weight Loss of the scaffolds

In vitro biodegradation studies were performed in test tube containing 4 mL of a PBS solution (pH 7.4) and this process was followed by an incubation for 35 d at 37 °C. Using same weight of material for each test and each day (W0, 20 mg) degradation of the samples was measured for certain days (1, 3, 5, 7, 14, 21, 28, and 35). On each day, related samples were removed from PBS medium, washed with pure water and dried in a vacuum oven for 24 h and the weighted (Wf). The dry weight of the samples was calculated as follows.

$$\% \text{ Weight Loss} = 100\ (W_f - W_0) / W_0$$

2.4.5. Chemical and thermal analysis of the scaffolds

Molecular structure and chemical identity of the scaffolds was evaluated using a Fourier-Transform Infrared Spectroscopy (FTIR, 4600 Jasco, Japan). The transmittance was evaluated in the wave number range from 4000 to 450 cm^{-1}. Attenuated total reflection (ATR) was utilized to obtain more precise peaks and 16 scans were run for each test.

Differential Scanning Calorimetry (DSC) test was used for each scaffold along with the PLA polymer to display their thermal behaviour and analyse their thermal properties such as glass transition temperatures (Tg) and melting temperature (Tm) using Perkin-Elmer Thermal

Analyzer System (PerkinElmer Inc., Mass., USA) equipped with Jude DSC system. Tests were carried out under an argon atmosphere (20 mL/T flow rate) with a scanning rate of 10 °C/min between 22 °C and 250 °C. All data were evaluated after the measurements with Pyris software (PerkinElmer Inc., Mass., USA) to measure Glass transition (Tg) and melting (Tm) temperatures.

2.4.6. Antibacterial properties of the scaffolds

Antibacterial potential of the samples were carried out by a disk diffusion method against Gram negative (*E. coli*) and Gram positive (*S. aureus*) bacterial strains. Luria Bertani (LB) agar was used as the medium for the bacteria. A bacterial suspension of each bacteria was spread on the agar plates. Each sample were placed on agar and incubated at 37 °C for 24 h. The antibacterial activity was determined through measurement of the diameter of the inhibition zone around the sample.

2.4.7. Cellular behaviour of scaffolds

The cellular behaviour of the scaffolds was also revealed using Saos-2 (human osteosarcoma) cells using MTT protocol [31] and results were evaluated for 24 h, 48 h and 72 h. Comprehensive details of the investigation are explained as a supplementary data section.

3. Results and discussion

Not only mechanical properties of the scaffolds, but morphological integrity is also known for having a direct influence on the permeability to allow diffusion of the nutrients for cells to survive and affecting the cellular response by providing better volume to surface area ratios [32]. Therefore, as one of the most crucial characterization type in order to assess and verify real life practicability of the scaffold materials produced morphological characterization of the 3D bioprinted scaffolds was comprehensively conducted. A wide variety of geometries can be established during bioprinting due to many factors that either can be organized such as environmental parameters or can't be controlled like properties of the materials used. Therefore, scaffold geometry including the sizes and orientation of the pores becomes very important, and these features can be directly related to the above-mentioned characteristics of the scaffolds. Scaffold morphology was determined using SEM imaging. Fig. 2 (a-f) shows the SEM images of each scaffold sample produced in this study. Morphology of the PLA/β-TCP group which is a combination of a synthetic polymeric phase and a ceramic phase resulted with square-shaped pores with orthogonal configuration. After adding different hydrogels to blend solution, the shape of the pores slightly shifted into more cylindrical shape peaking to its highest with the chitosan including samples. Even though the scaffolds are being produced with 3D bioprinting system which can provide total control over the scaffold morphology, constant environmental conditions such as temperature, pressure, evaporation rate and even gravity can affect the solidification process if the solutions have different viscosity, density and surface tension ratios depending of the only variable which is possessing different types of materials within the scaffolds. Therefore, it can be reported that the results varied depending on the material type used within the scaffolds since the other conditions were kept the same during bioprinting. Compared to the other pore types such as gyroid and gyroid like structures, rectangular pores are reported to demonstrate higher mechanical properties and better permeability [33]. This cylindrical shape can increase the surface area of the pores and can be beneficial for the biocompatibility than the rectangular shape. However, the proliferation of the different type of cells may be affected with various factors. Therefore, scaffold morphology can give pioneer information about future characteristics of the scaffolds and can be guided with the aim of the desired tissue engineering application.

The pore size of the scaffolds and their distribution is also an essential morphological feature since the natural phenomenon called cell seeding and migration are being provided through those pores as well as the physiological and biochemical mechanisms like exchanging waste and nutrients between cells and tissues [34]. Previous studies comparing the characteristics of the isotropic and the gradient pore size distribution was reported that the isotropic pore size distribution can lead to uniform and homogenous distribution of the cells being seeded on the scaffolds which can facilitate the cell seeding mechanism on the scaffolds and eventually increase the biocompatibility. Additionally, larger pore sizes are reported to be linked to increased cell accumulation [35]. Therefore, decreasing the range of the pore size distribution and providing the largest pore size diameter available without compromising morphological integrity of the scaffolds can be promising to achieve highest cellular response with most significant cell seeding and adhesion where the sufficient amount of proliferation is available by high biocompability. Therefore, scaffolds produced by biocompatible materials should possess above mentioned

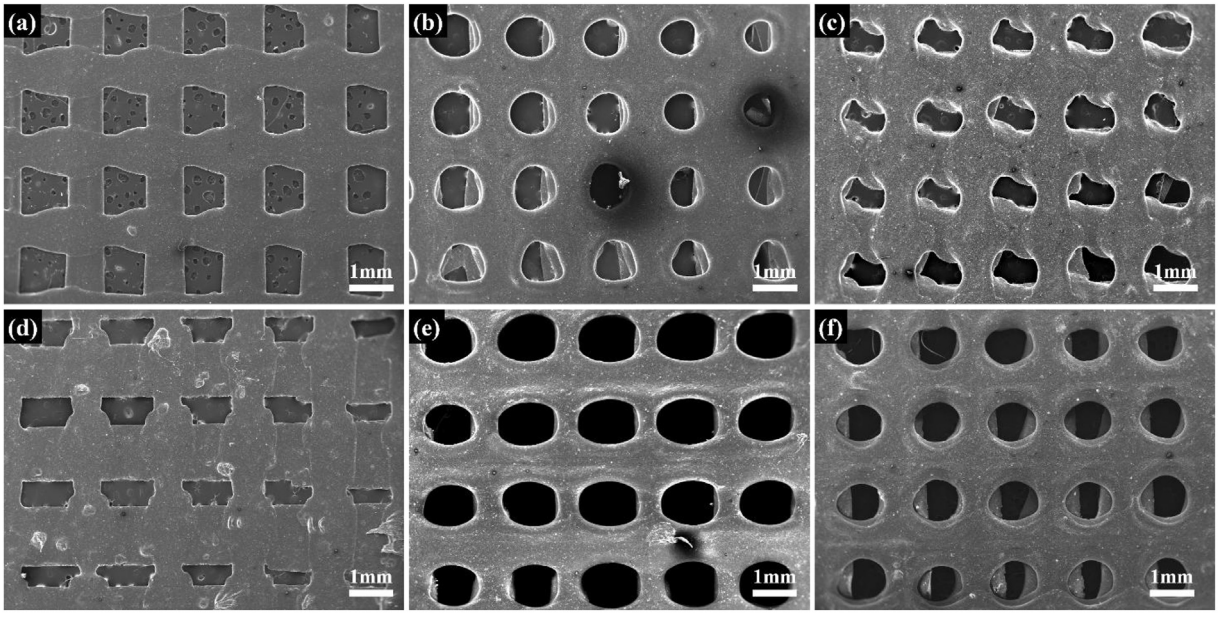

Fig. 2. SEM images of the 3D Bioprinted PLA/β-TCP scaffolds with different hydrogel content. (a) without hydrogel, (b,c,d,e) Col, HLh, Salg, Ch hydrogels respectively, (e) AMX added scaffolds.

features in order to benefit from the biocompatible characteristics of the material used which means a proper cellular response can only be achieved by combining a balance between material wise and scaffold wise characteristics. After the bioprinting pore size frequency and differences were also measured and shown in Fig. 3(a-f). Results indicated that average pore size distributions of PLA/β-TCP scaffolds resulted 1.23 mm, maximum was measured 1.35 mm, minimum was resulted in 1.05 mm. After addition of the Col, SAlg, HLh, Ch and Ch/AMX, average size of the pores was resulted 0.90 mm, 0.99 mm, 1.09 mm, 1.23 mm and 0.97 mm respectively. Maximum pore size measured resulted with 1.29 mm, 1.11 mm, 1.32 mm, 1.39 mm and1.13 mm respectively. However, minimum pore size values was observed 1.09 mm, 0.75 mm, 0.86 mm, 1.10 mm, 0.81 mm respectively. Studies have been reported on tissue engineering that the pore sizes are required to be at least 0.3 mm in order to ensure sufficient permeability [36]. Therefore, since our scaffolds are beyond that requirement, material exchange can be provided on the scaffolds without any limitations. Most isotropic pore size distribution and the largest average and maximum pore diameters size was observed for the chitosan hydrogel including samples. During the bioprinting, environmental conditions and bioprinting speed were kept constant for each sample. Therefore, pore size differences can be related (1)with the types of materials into the composite structure and (2) with the solution properties such as viscosity, surface tension and density provided by different hydrogels added to the PLA/β-TCP blends.

Solution properties are also important factors during bioprinting due to similarity of the concentrations and types of the materials used, solution properties are resulted similar for each sample but the chitosan including samples. This might be due to addition of DMSO which increase the viscosity and surface tension of the solutions. However, due to the convenience of using highly evaporable solvent, solution properties can be considered as a key point to determine whether the prepared solution is printable or not, since the extreme conditions tend to limit or cease constant flow of the solution to the nozzle tip and eventually interrupting the bioprinting. In addition to that, solidification process can be easily controlled by heating the build table, allowing the solutions with low viscosity to be printed without any problems. Solution properties prior to 3D bioprinting are given in Table 1. The viscosity of the solutions before bioprinting was measured between 768 and 950 cP, the surface tension was measured 52.84–65.75 mN/m and eventually, the density of the samples was measured between 1.29 and 1.32 mN/m.

Since the higher porosity or the varying features of the pores can alter the surface area per unit volume, biodegradation kinetics of the scaffolds

Table 1
Solution properties before 3D bioprinting.

Solution Contents	Viscosity (cP)	Surface Tension (mN/m)	Density (g/ml)
PLA/β-TCP	805 ± 12	57.48 ± 2.37	1.30 ± 0.05
PLA/β-TCP/Col	768 ± 29	55.52 ± 2.29	1.23 ± 0.03
PLA/β-TCP/HLh	875 ± 22	54.23 ± 2.27	1.32 ± 0.02
PLA/β-TCP/SAlg	800 ± 12	52.84 ± 2.37	1.29 ± 0.07
PLA/β-TCP/Ch	950 ± 29	60.22 ± 2.29	1.30 ± 0.12
PLA/β-TCP/Ch/AMX	942 ± 22	65.75 ± 2.23	1.32 ± 0.03

can be influenced by these factors. Not only limited with that, biodegradation is also directly related with the characteristics of the materials and can be affected by their co-existence within the composite structures. Simultaneous biodegradation along with the ongoing cell proliferation is one of the most important requirement of a successful tissue scaffold since the transition will enable cells to be replaced with the scaffolds in order to achieve desired tissue regeneration. Scaffolds prepared in our study was mainly consisted by PLA which can be degraded into a form of lactic acid and the mechanism can be explained by a random hydrolysis of their ester bonds which is a routine biochemical activity within the living organism. Therefore, this degradation process is expected to be friendly and nontoxic to the host tissue [37]. However, slow degradation speed of PLA can create limitations to practicability of the scaffolds and this handicap is relatively compensated with β-TCP which is reported to increase the biodegradability of the PLA as described in the previous studies [38]. Degradation graph of the scaffolds is displayed in Fig. 4. PLA/β-TCP scaffolds displayed almost 3.8% degradation over the period of 35d while the hydrogels containing samples were pushed up to 5%. Highest degradation rate was observed for Ch containing scaffolds. This outcome can be related with few reasons such as high biological features of the material or the chemical bonding differences during the hydrogel forming mechanism of each material. Presence of the AMX was not able to affect the degradation and results were similar to the other scaffolds. This study revealed that the presence of the hydrogels is also slightly affect the biodegradation behaviour of the scaffolds, even though crosslinking is an important factor for decreasing the degradation rate of the collagen hydrogels and they possess small quantities within the structure [39]. For each sample tests in our study, biodegradation rate is higher than previous similar reports, showing the biodegradation of PLA, β-TCP and their composite forms [40]. This can be mainly related with the porous structure of the tissue scaffolds as a result of possessing high

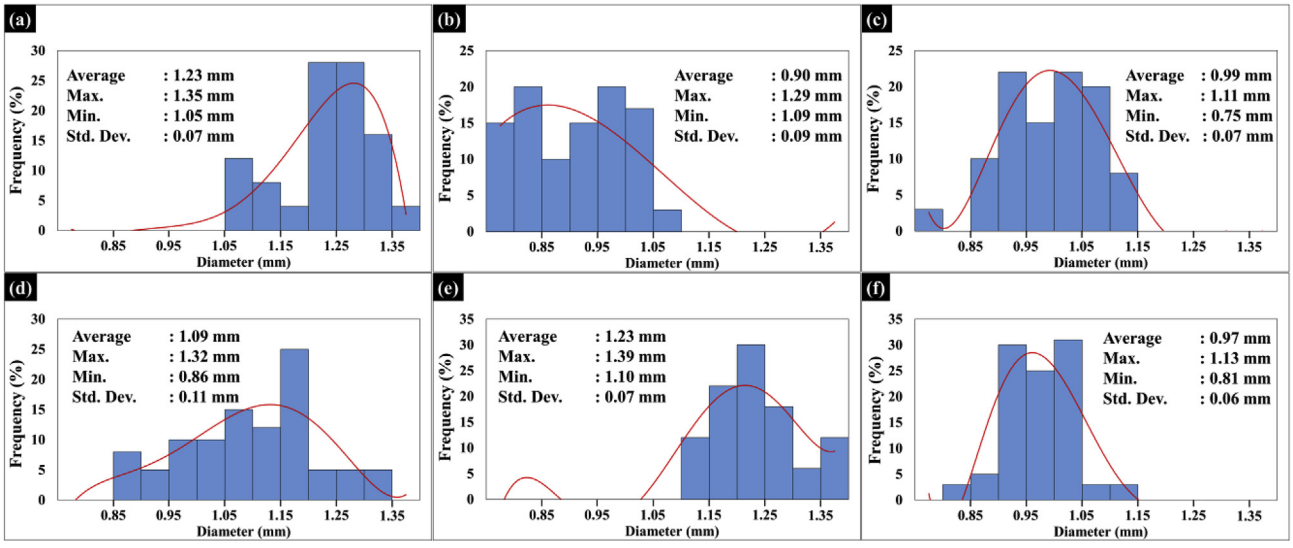

Fig. 3. Pore size distribution frequency of the PLA/β-TCP scaffolds. PLA/β-TCP scaffold samples with different hydrogel contents (a) no hydrogel (b) Col, (c) HLh, (d) SAlg, (e) Ch, (f) Ch/AMX.

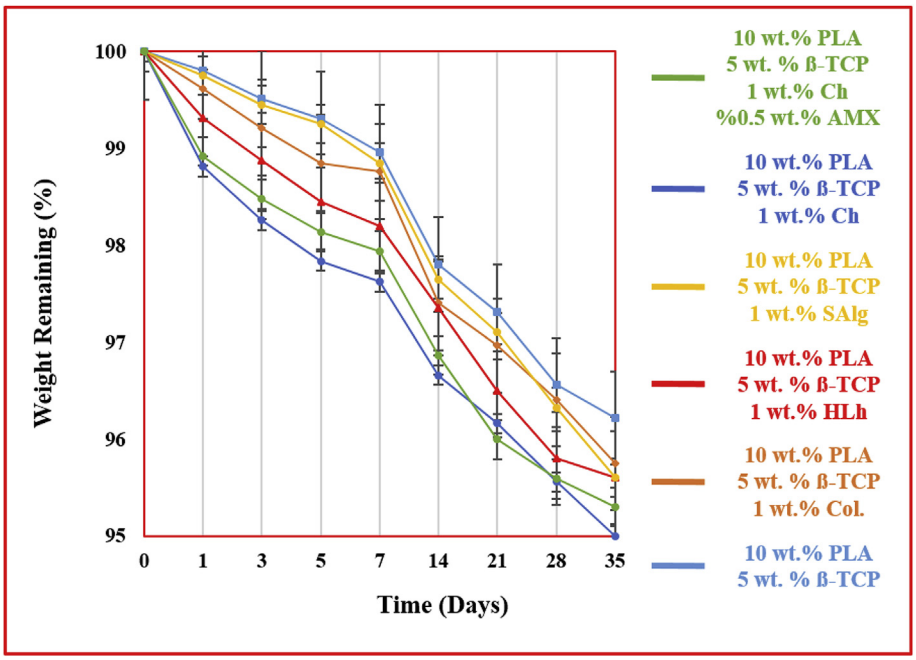

Fig. 4. Diagram of the biodegradation behaviour of the scaffolds over 35 d.

surface area can be also associated with proper simulation of the imitational body conditions during the experiment.

The chemical identity of the scaffolds revealed using FTIR-ATR, and the graphical illustration of results is shown in Fig. 5. Characteristic bands of PLA were observed at 1742 cm^{-1}, which can be recognized as backbone ester group of PLA. The —C—O— stretching vibration regarding the ester units related with the molecular structure of PLA was observed at 1074-1177 cm^{-1}. A tiny but another characteristic peak indicates that the —OH of L-lactic acid is revealed at 3640 cm^{-1} [41,42] Additionally, the presence of the β-TCP was manifested by the peaks at 1019 cm^{-1}, 603 cm^{-1} and 565 cm^{-1} [43]. On the other hand, peaks of the hydrogels were also revealed within the scaffolds. For collagen, at 1647 cm^{-1} C═O stretching which can be attributed to the major characteristic of the amide I band was observed. Following that, Amide A band position was located at 3342 cm^{-1} as —OH vibrations and NH stretching at 3013 cm^{-1} corresponded to the Amide B bands. COO symmetrical stretching of the collagen was also located at 1074 cm^{-1} but overlapped with the backbone ester group of PLA peaks [16,44]. Peaks of the HLh such as hydroxyl (OH) stretching vibration manifested ad 3340 cm^{-1} and carbon–hydrogen (C—H) stretching vibration located as a weak peak at 2913 cm^{-1} [45]. Due to the low ratio of the HLh in the composite structure, rest of the peaks overlapped with other materials and did not demonstrate a significant difference. As another type of hydrogel used in this study to enhance the properties of the scaffolds, SAlg demonstrated characteristic absorption bands at 3340 cm^{-1}, manifesting a large and broad peak representing the hydroxyl groups (—OH). Asymmetric bending vibrations of N—H groups located within the SAlg was exhibited with a significant peak at 1585 cm^{-1}. N—H stretching peaks was observed at 1443 cm^{-1} and 1376 cm^{-1} [46,47]. Ch related peaks were found at 3390 cm^{-1}, 2860 cm^{-1}, 1631 cm^{-1}, 1560 cm^{-1} and 890 cm-1 representing the O—H stretching, C—H vibration, primary amide H—N—H vibration and pyranoid ring stretching respectively [48] Finally, AMX was manifested several but very weak peaks between 2880 cm^{-1} - 3400 cm^{-1} and few strong peaks at 1676 cm^{-1}, 1566 cm^{-1} and 1239 cm^{-1} [49].

Because of each scaffold mainly consisted by PLA and β-TCP, peaks of those materials were frequently observed in each sample and typical differences observed between different hydrogel types within the

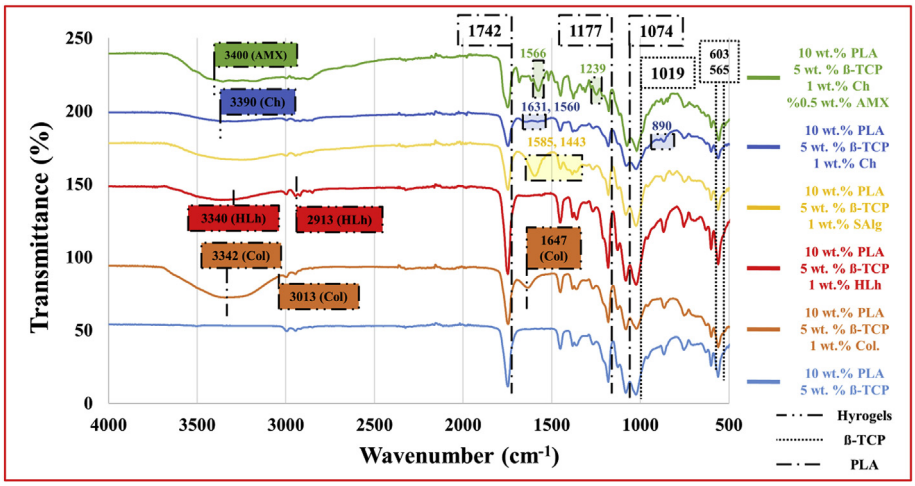

Fig. 5. FTIR spectra of the 3D bioprinted scaffolds.

scaffolds. Due to the similar bonds between materials, overlaps were also occurred. HLh is a material that is not widely studied yet. Therefore, their chemical behaviour and bonds are yet to be revealed compared with other hydrogel types used in this study. However, there are main characteristics peaks of the HLh was able to be located. Due to overlaps and cross linking process of the hydrogels and their low ratio within the scaffold structure, some of the peaks were seemed to be slightly shifted from their original locations reported in the related literature. However, all materials were demonstrated peaks in order to prove their presence within the scaffold materials.

To determine the thermal dynamics generated by the interactions between materials used during production of the scaffolds while revealing the critical temperature values such as melting temperature (Tm) and glass transition temperature (Tg), DSC was used. Fig. 6 representing the thermal behaviour of the scaffolds, revealing the critical temperatures for each sample type. Results indicated that the, Tg and Tm of the pure PLA was observed 70 °C and 160 °C respectively. Compared to that, key temperatures were decreased for PLA/β-TCP blend and measured 58 °C for Tg and 147 °C for Tm. After adding the other materials, these key temperatures shifted with a small increase without making any significant change. Outcomes of the DSC studies can be explained with the thermal behaviour of PLA which has the highest ratio within the scaffolds structure compared with the other types of materials used in this study. Therefore, Tg and Tm values of each scaffold was resulted not very far away from the pure PLA characteristics. However, interaction of the materials with the PLA polymer chains was shifted to thermal key temperatures. Furthermore, the shift in Tm and Tg values to lower temperatures can be explained by the difference of bonding interactions between the molecules in the PLA chains by other materials. This inhibition is caused by the fact that other materials within scaffold structure enter the parts where bonds are located and cause differences in their interaction level and strength. The melting temperature therefore showed a decrease, the same phenomenon is also applied for the glass transition temperature, and amount of heat required for the formation of segmental movements in PLA polymer was reduced by the materials used since the energetic interaction at the level of these bonds causes the need to consume less energy to defeat the total forces between the bonds and change the crystallization [24,50]. In addition, a single Tm and Tg value for each sample can be shown as evidence for unique and homogenous structure consisted by different materials within the scaffolds.

Another important step is to achieve the mechanical properties of the scaffolds The compressive strength of the scaffolds produced in this study was measured between 1.2 and 1.5 MPA and shown in Table 2.

Table 2
Mechanical test results of the scaffold samples.

Scaffold Structure	Compressive Strength (MPa)
PLA/β-TCP	1.59 ± 0.43
PLA/β-TCP/Col	1.38 ± 0.22
PLA/β-TCP/HLh	1.54 ± 0.25
PLA/β-TCP/SAlg	1.49 ± 0.75
PLA/β-TCP/Ch	1.29 ± 0.23
PLA/β-TCP/Ch/AMX	1.24 ± 0.53

Results varied between 1.24 and 1.59 MPa. After the addition of the materials into the PLA/β-TCP phase, mechanical properties were tending to decrease. Previous studies using PLA and β-TCP reported that the compressive strength of the scaffolds with low porosity using different fabrication method compared to our study was resulted between 17.8 and 35.7 MPa. On the other hand, as the porosity increases, this value was significantly decreased and reported within the range of 1–3 MPa depending on the concentration ratios of the materials [38]. Therefore, in our study, porosity led the compressive strength to be decreased compared to the literature and since the hydrogels within the composite consisted by a small portion of the material ratio and compressive strength was on only affected with a slight decrease.

Antimicrobial activity is also important factor since infections caused by invasion of the pathogens can slow down the healing of related tissue. Therefore, antibacterial activity of the scaffolds was assessed using *Escherichia* coli as gram-negative bacteria and *Staphylococcus aureus* as gram-positive bacteria in order to compare scaffolds against both kind of bacteria strains and results are shown in Fig. 7. Except the Ch and AMX including samples, scaffolds were not able to demonstrate antimicrobial activity. This can be related to the already known antibacterial properties of the Ch and it is also one of the main differences among the other hydrogels used in this study [26]. Results indicated that the diameters of inhibition zone versus *Escherichia* coli of the samples are approximately 20 mm and 16 mm for Ch/AMX and Ch, respectively. Similar to the results obtained from Gram-negative bacteria, the inhibition zone versus *Staphylococcus aureus* is approximately 18 mm and 11 mm, respectively.

Results also suggesting that AMX can be used as an effective antibacterial agent on both grams positive and gram negative bacteria to increase antimicrobial activity of chitosan. This data point out that AMX and Ch mixture has a synergistic antimicrobial effect on both Gram

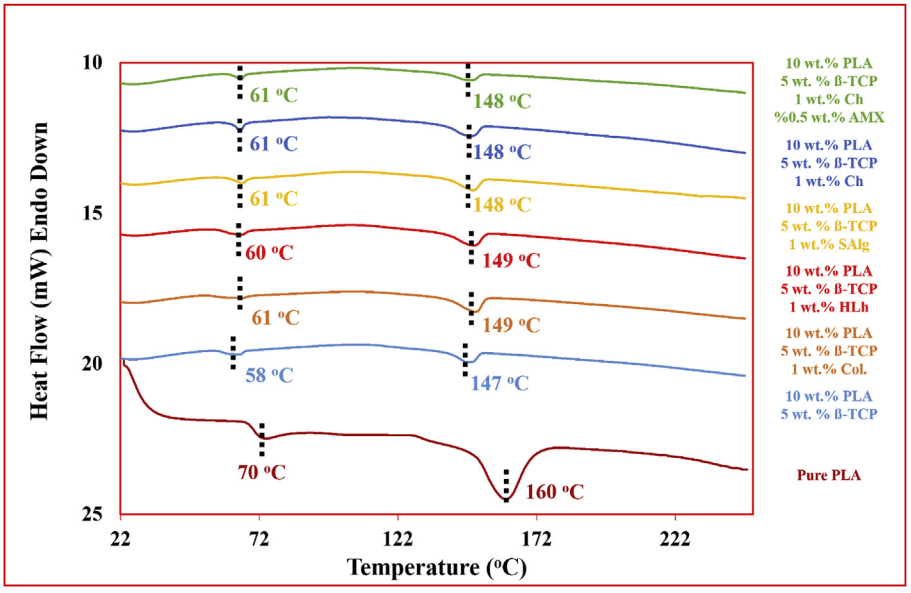

Fig. 6. DSC thermographs of the scaffolds.

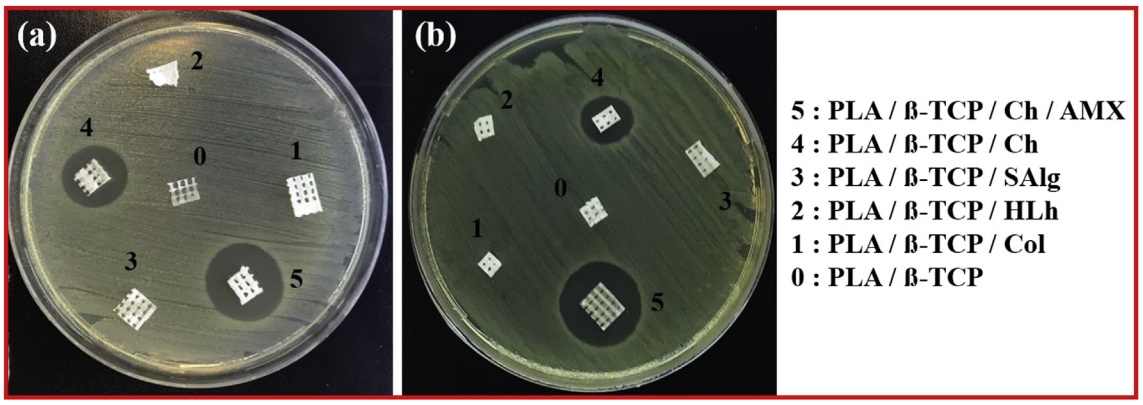

Fig. 7. Antibacterial activity of samples with inhibition zones against (a) *E. coli* and (b) *S. aureus*.

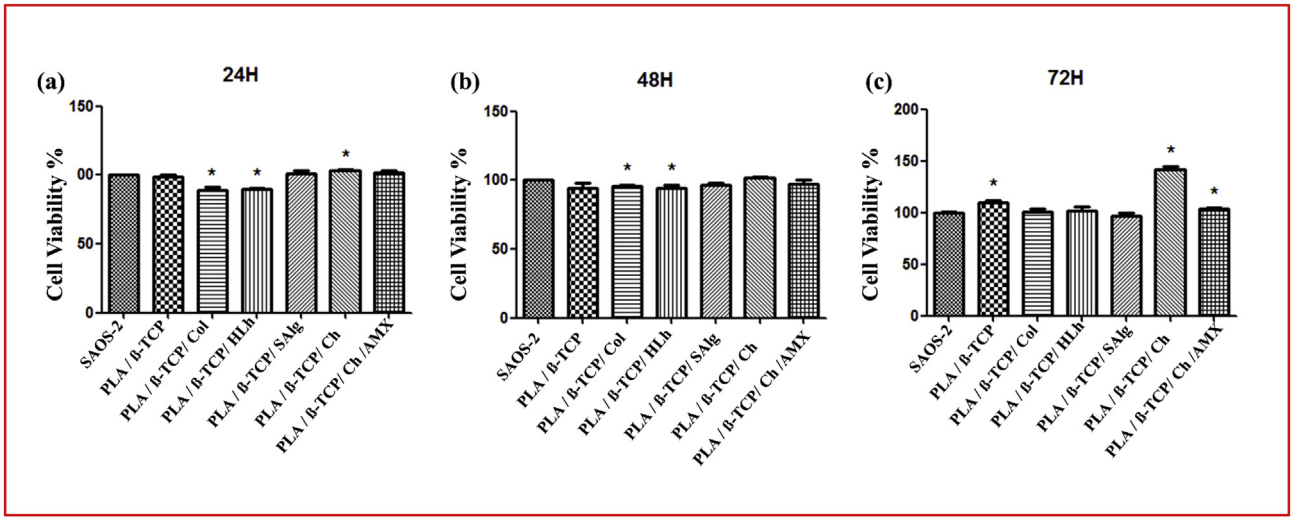

Fig. 8. MTT cell viability assays of the scaffolds for (a) 24, (b) 48, (c) 72 h.

positive and negative bacteria. Compared to the other studies reporting the production of the 3D scaffolds with antibacterial properties, our results demonstrated better inhibition zones.

In order to ensure the practicability of the scaffolds, revealing the cellular interactions between cells and scaffolds is a crucial step since the tissue regeneration through scaffolds is a concept which is directly related with biocompability. Therefore, certain factors such as being non-toxic and exhibiting good cell attachment, proliferation, and differentiation are essential parameters to prepare biocompatible scaffolds [51]. To investigate these properties, MTT assay was performed. Cytotoxicity (MTT) tests indicated that scaffolds exhibited no cytotoxic activity and interaction between cells and scaffold is promising as demonstrated in Fig. 8. However, since the PLA/β-TCP matrix is the common content of each scaffold, reason of the different biocompatibility levels can be related to the type of hydrogel within the scaffold. Cell viability was observed increasing between consecutive days. Among others, metabolic activity was highest on Ch with highest cell adhesion, and that is being followed by HLh. Another important fact, which needs to be underlined, is the cell adhesion ratio of the PLA/β-TCP matrixes, which doesn't have any hydrogel content within.

Those scaffolds were suffered by decreased cell adhesion like 5–10% compared to the control group. This status proves that the cell adhesion is highly influenced by the biocompatibility of the hydrogels. However, Ch including samples was shown not only good adhesion but also exhibited significant proliferation and cell viability resulted with 150%. However, the addition of the AMX inhibited the cell viability almost 40%, which might be due to the cytotoxicity induced by the AMX As a result, obtained data from MTT test confirms that the scaffolds produced in this study were highly biocompatible. Furthermore, cellular behaviour and their interaction with the scaffolds with different hydrogel contents was also observed with SEM imaging and shown in Fig. 9. After 24 h, 48 h and 72 h of incubation, samples were analysed. Appropriate cell adhesion, proliferation and spreading among the scaffold were observed. After 24 h, younger cells were found mostly in the shape of an orbicular at the surface of the scaffolds. Even though they were attached to the surface, no roots or any positive sign of adhesion was observed. However, after 48 h, cells were started to increase their contact area with the scaffolds, began to invade the scaffolds with their extensions which can be considered as a good sign of biocompatibility.

Finally, after being incubated for 72 h, scaffolds were utterly invaded with mature cells both embed and adhered to the surface with many extensions and with their increased sizes. Results also indicated that the, cellular behaviour and positive signs of biocompatibility as proliferation and adhesion was observed on all samples and peaking at the presence of Ch hydrogel. However, addition of the AMX not only failed to contribute those attributes but also decreased the signs of biocompatibility of the scaffolds with the terms of above mentioned features. Therefore, it can be said that addition of the Ch into the scaffold structure influenced the cellular behaviour significantly and using antibiotics like AMX needs to be considered carefully depending on aim and usage of scaffolds.

4. Conclusion

In this study, PLA/β-TCP scaffolds were produced solely as a control

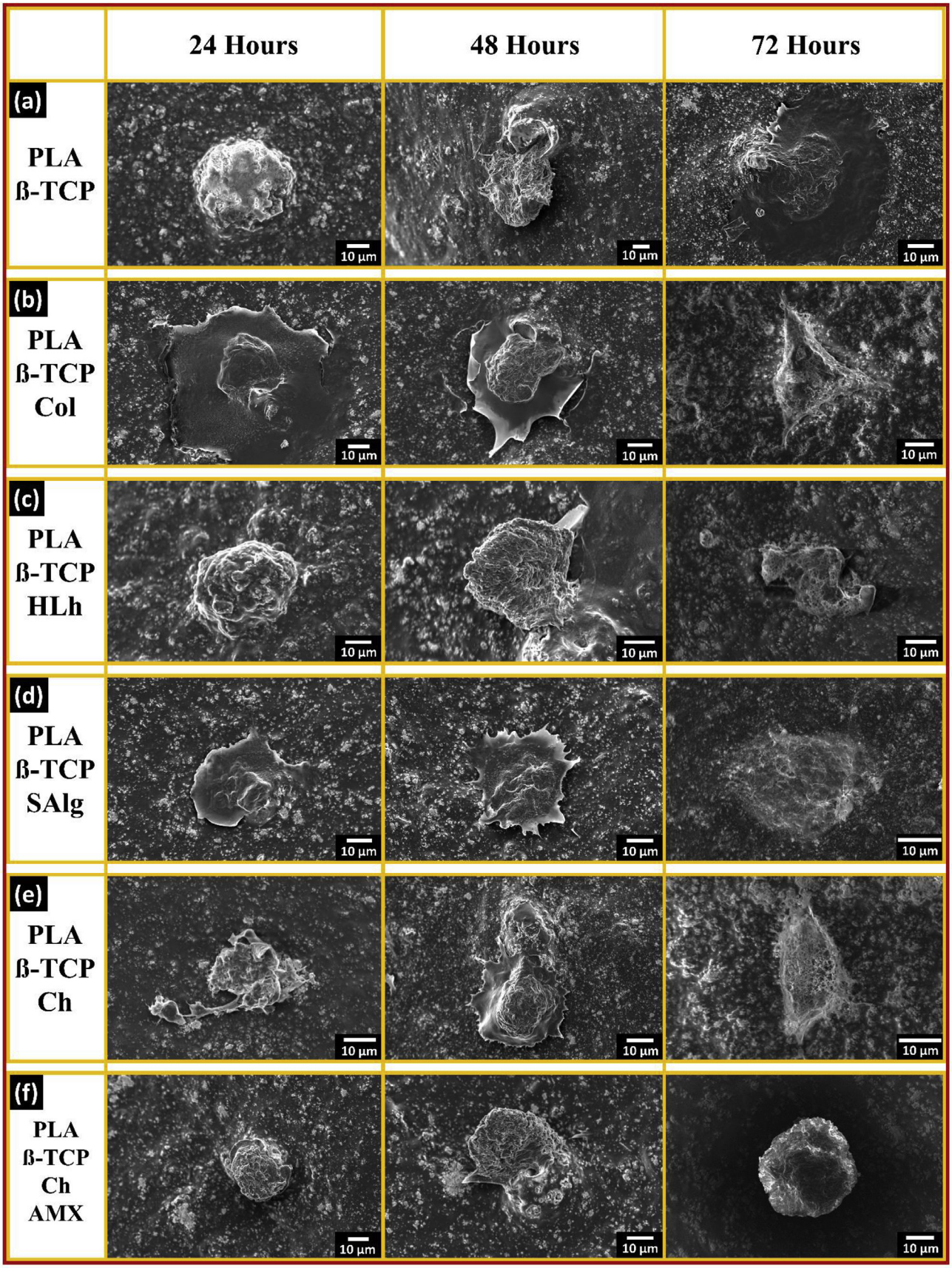

Fig. 9. Scanning electron microscope images of PLA/β-TCP scaffold samples with different hydrogel contents (a) no hydrogel (b) Col, (c) HLh, (d) SAlg, (e) Ch, (f) Ch/AMX after incubation period of 24, 48 and 72 h.

group and with addition of four different hydrogels namely collagen, halamonas levan, sodium alginate and chitosan in order to analyse their influence on the mechanical, chemical and antibacterial properties of the scaffolds as well as the cellular behaviour which were comprehensively investigated and demonstrated. Compared to the other hydrogel types, Ch enhanced the scaffolds with the most significant outcomes in term of scaffold morphology and cell viability. Using amoxicillin as an antibacterial material with the purpose of inducing an antibacterial effect of the scaffold was successfully implemented to the scaffolds. However, presence of the amoxicillin affected the cell viability. As conclusion, scaffold samples consisted by incorporation of PLA/β-TCP/Ch looks promising to be used as tissue scaffolds with their significant cell viability, strong antibacterial properties and durable mechanical features such as compressive strength and proper porosity.

Acknowledgements

This study has been founded by BAPKO, Marmara University; grant no: FEN-C-YLP-150218-0053.

References

[1] U.S. Department of Health and Human Service. Donate the Gift of Life, 2013.
[2] R. Langer, J.-P. Vacanti, Tissue engineering, Science 260 (1993) 920.
[3] L.-G. Griffith, M.A. Swartz, Capturing complex 3D tissue physiology in vitro, Nat. Rev. Mol. Cell Biol. 7 (2006) 211.
[4] S. Wu, X. Liu, K.W.K. Yeung, C.S. Liu, X.J. Yang, Biomimetic porous scaffolds for bone tissue engineering, Mater. Sci. Eng. R. 80 (2014) 1.
[5] B.P. Chan, K.W. Leong, Scaffolding in tissue engineering: general approaches and tissue-specific considerations, Eur. Spine J. 17 (2008) 467.
[6] R. Nazarov, H.J. Jin, D.L. Kaplan, Porous 3-D scaffolds from regenerated silk fibroin, Biomacromolecules 5 (2004) 718.
[7] J. Lannutti, D. Reneker, T. Ma, D. Tomasko, D. Farson, Electrospinning for tissue engineering scaffolds, Mater. Sci. Eng. C 27 (2007) 504.
[8] M.O. Aydogdu, N. Ekren, O. Kilic, F.N. Oktar, O. Gunduz, 3D liquid bioprinting of the PCL/ß-TCP scaffolds, Mater. Sci. Forum 923 (2018) 79.
[9] S.-M. Peltola, F.P.W. Melchels, D.W. Grijpma, M. Kellomaki, A review of rapid prototyping techniques for tissue engineering purposes, Ann. Med. 40 (2008) 268.
[10] A. Standard, F2792, Standard Terminology for Additive Manufacturing Technologies, ASTM International, West Conshohocken, Pa, USA, 2012.
[11] S.T. Ozak, P. Ozkan, Nanotechnology and dentistry, Eur. J. Dermatol. 7 (2013) 145.
[12] K.C. Dee, D.A. Pulelo, R. Bizios, An Introduction to Tissue Biomaterial Interactions, Wiley-Liss, Publications, Hoboken, NJ, 2002.
[13] M. Sittinger, J. Bujia, W.W. Minuth, C. Hammer, G.R. Burmester, Engineering of cartilage tissue using bioresorbable polymer carriers in perfusion culture, Biomaterials 15 (1994) 451.
[14] J.R. Porter, T.T. Ruckh, K.C. Popat, Bone tissue engineering: a review in bone biomimetics and drug delivery strategies, Biotechnol. Prog. 25 (2009) 1539.
[15] S.V. Nolte, W. Xu, H.O. Rennekampff, H.P. Rodemann, Diversity of fibroblasts–a review on implications for skin tissue engineering, Cells. Tissues. Organ 187 (2008) 165.
[16] M.O. Aydogdu, J. Chou, E. Altun, N. Ekren, S. Cakmak, M. Eroglu, A.A. Osman, Production of the biomimetic small diameter blood vessels for cardiovascular tissue engineering, Int. J. Polym. Mater. Po. 1 (2018).
[17] R.M. Rasal, A.V. Janorkar, D.E. Hirt, Poly(lactic acid) modifications, Prog. Polym. Sci. 89 (2009) 252.
[18] J. Li, W. Zheng, Y. Zheng, X. Lou, Cell responses and hemocompatibility of g-HA/PLA composites, Sci. China Life Sci. 54 (2011) 366.
[19] J. Suganuma, H. Alexander, Biological response of intramedullary bone to poly-L-lactic acid, J. Appl. Biomater. 4 (1) (1993) 13–27.
[20] X. Li, H. Liu, X. Niu, Y. Fan, Q. Feng, F.Z. Cui, F. Watari, Osteogenic differentiation of human adipose-derived stem cells induced by osteoinductive calcium phosphate ceramics, J. Biomed. Mater. Res. *B.* 97 (1) (2011) 10.
[21] R.E. Holmes, R.W. Bucholz, V. Mooney, Porous hydroxyapatite as a bone-graft substitute in metaphyseal defects. A histometric study, J. Bone. Joint. Surg. Am. 68 (6) (1986) 904.
[22] M.W. Tibbitt, K. S, Hydrogels as extracellular matrix mimics for 3D cell culture, Anseth. *Biotechnol. Bioeng* 103 (2009) 655.
[23] P. Fratzl, Collagen: Structure and Mechanics, Springer, New York, 2008.
[24] M.S. Bostan, E.C. Mutlu, H. Kazak, S.S. Keskin, E. Toksoy-Oner, M.S. Eroglu, Comprehensive characterization of chitosan/PEO/levan ternary blend films, Carbohydr. Polym. 102 (2014) 993.
[25] B. Kulseng, G. Skjåk-Bræk, L. Ryan, A. Andersson, A. King, A. Faxvaag, T. Espevik, Transplantation of alginate microcapsules: generation of antibodies against alginates and encapsulated porcine islet-like cell clusters, Transplantation 67 (1999) 978.
[26] W. Qinghua, M. Marion, L. Sophie, T. Daniel, H. Marie-Claude, 3D printing of microstructured and stretchable chitosan hydrogel for guided cell growth, Adv. Biosys. 1 (2017) 1700058.
[27] J.O. Hollinger, An Introduction to Biomaterial, second ed., CRC Press, Taylor & Francis, 2011.
[28] J. Berger, M. Reist, J.M. Mayer, O. Fel, N.A. Peppas, R. Gurny, Structure and interactions in covalently and ionically crosslinked chitosan hydrogels for biomedical applications, Eur. *J. Pharm. Biopharm.* 57 (2004) 19.
[29] S. Wang, F. Zheng, Y. Huang, Y. Fang, M. Shen, M. Zhu, X. Shi, Encapsulation of amoxicillin within laponite-doped poly(lactic-co-glycolic acid) nanofibers: preparation, characterization, and antibacterial activity, ACS Appl. Mater. Interfaces 4 (2012) 6393.
[30] K. Songsurang, J. Pakdeebumrung, N. Praphairaksit, N. Muangsin, Sustained release of amoxicillin from ethyl cellulose-coated amoxicillin/chitosan-cyclodextrin-based tablets, AAPS. Pharm. Sci. Tech. 12 (2011) 35.
[31] T. Mosmann, Rapid colorimetric assay for cellular growth and survival: application to proliferation and cytotoxicity assays, J. Immunol. Methods 65 (1983) 55.
[32] M. Charles-Harris, M.A. Koch, M. Navarro, D. Lacroix, E. Engel, J.A.A. Planell, A PLA/calcium phosphate degradable composite material for bone tissue engineering: an in vitro study, *J. Mater. Sci. Mater.* Med. 19 (2008) 1503.
[33] D. Ali, S. Sen, Finite element analysis of mechanical behavior, permeability and fluid induced wall shear stress of high porosity scaffolds with gyroid and lattice-based architectures, J. Mech. Behav. Biomed. Mater. 75 (2017) 262.
[34] E. Díaz, I. Sandonis, M.B. Valle, In Vitro degradation of poly(caprolactone)/nHA composites, J. Nanomater. 802435 (2014) 8.
[35] F.P. W Melchels, B. Tonnarelli, A.L. Olivares, I. Martin, D. Lacroix, J. Feijen, D.J. Wendt, D.W. Grijpm, The influence of the scaffold design on the distribution of adhering cells after perfusion cell seeding, Biomaterials 32 (2011) 2878.
[36] D.W. Hutmacher, J.T. Schantz, C.X. F Lam, K.C. Tan, T.C. Lim, State of the art and future directions of scaffold-based bone engineering from a biomaterials perspective, J. Tissue Eng. Regenerat. Med. 1 (2007) 245.
[37] P.A. Guntillake, R. Adhikari, Biodegradable synthetic polymers for tissue engineering, Eur. Cells Mater. 5 (2003) 1.
[38] L. Cao, P.G. Duan, H.R. Wang, X.L. Li, F.L. Yuan, Z.Y. Fan, S. M Li, J. Dong, Degradation and osteogenic potential of a novel poly(lactic acid)/nano-sized β-tricalcium phosphate scaffold, Int. J. Nanomed. 7 (2012) 5881.
[39] K.A. Alberti, Q. Xu, Biocompatibility and degradation of tendon-derived scaffolds, Regen. Biomater. 3 (2016) 1.
[40] P. Kucharczyk, A. Pavelková, P. Stloukal, V. Sedlarík, Degradation behaviour of PLA-based polyesterurethanes under abiotic and biotic environments, Polym. Degrad. Stabil. 129 (2016) 222.
[41] C.C. Chen, J.Y. Chueh, H. Tseng, H.M. Huang, S.Y. Lee, Preparation and characterization of biodegradable PLA polymeric blends, Biomaterials 24 (2003) 1167.
[42] X.P. Wei, Y.L. Luo, F. Xu, Y.S. Chen, Sensitive conductive polymer composites based on polylactic acid filled with multiwalled carbon nanotubes for chemical vapor sensing, Synth. Met. 2 (2016) 216.
[43] D.S. Tavares, L. O Castro, G.D. A Soares, G.G. Alves, J.M. Granjeiro, Synthesis and cytotoxicity evaluation of granular magnesium substituted β-tricalcium phosphate, Appl. Oral. Sci. 21 (2013) 37.
[44] B.C. Vidal, M.L. Mello, Collagen type I amide I band infrared spectroscopy, Micron 42 (2011) 283.
[45] F. Kucukasik, H. Kazak, D. Güney, I. Finore, A. Poli, O. Yenigun, B. Nicolaus, E. Toksoy Oner, Olasses as fermentation substrate for levan production by Halomonas sp, Appl. Microbiol. Biotechnol. 89 (2011) 1729.
[46] R. Pereira, A. Tojeira, D.C. Vaz, A. Mendes, P. Bártolo, Preparation and characterization of films based on alginate and aloe vera, Int. J. Polym. Anal. Charact. 16 (2011) 449.
[47] M.G. Sankalia, R.C. Mashru, J.M. Sankalia, V.B. Sutariya, Reversed chitosan-alginate polyelectrolyte complex for stability improvement of alpha-amylase: optimization and physicochemical characterization, Eur. J. Pharm. Biopharm. 65 (2007) 215.
[48] S. Bashir, Y.Y. Teo, S. Naeem, S. Ramesh, K. Ramesh, pH responsive N-succinyl chitosan/Poly (acrylamide-co-acrylic acid) hydrogels and in vitro release of 5-fluorouracil, PLoS One 12 (2017), 0185505.
[49] D.M. Patel, D.K. Patel, C.N. Patel, Formulation and evaluation of floating oral in situ gelling system of amoxicillin, ISRN Dent 1 (2011).
[50] E.C. Mutlu, M.S. Bostan, F. Bahadori, A. Kocyigit, E. Toksoy Oner, M.S. Eroglu, Lecithin-acrylamido-2-methylpropane sulfonate based crosslinked phospholipid nanoparticles as drug carrier, J. Appl. Polym. Sci. 133 (2016) 44105.
[51] E. Altun, M.O. Aydogdu, F. Koc, M. Crabbe-Mann, F. Brako, R. Kaur-Matharu, G. Ozen, S.E. Kuruca, U. Edirisinghe, O. Gunduz, M. Edirisinghe, Macromol. Mater. Eng. 303 (2018) 1700607.